IP2016 / 4th International Workshop on Induced Polarization

Advances in spectral inversion of time-domain induced polarization

Gianluca Fiandaca
HydroGeophysics Group
Department of Geoscience
Aarhus University (Denmark)
gianluca.fiandaca@geo.au.dk

Esben Auken
HydroGeophysics Group
Department of Geoscience
Aarhus University (Denmark)
esben.auken@geo.au.dk

Anders Vest Christiansen
HydroGeophysics Group
Department of Geoscience
Aarhus University (Denmark)
anders.vest@geo.au.dk

SUMMARY

The extraction of spectral information in the inversion process of time-domain (TD) induced polarization (IP) data is changing the use of the TDIP method. Data interpretation is evolving from a qualitative description of the subsurface, able only to discriminate the presence of contrasts in chargeability parameters, towards a quantitative analysis of the investigated media, which allows for detailed soil- and rock-type characterization. In this work a review of the recent advances in spectral inversion of TDIP data is presented, in terms of: supported IP parameterizations; modelling of transmitter waveform; support for buried electrodes; model regularization; computation of the depth of investigation.
Keywords: spectral inversion, time-domain, Cole-Cole, CPA, transmitter waveform

INTRODUCTION

Recently, the interpretation and inversion of TDIP data has changed from only inverting for the integral changeability to consider also the spectral information contained in the IP response curves (Fiandaca *et al.*, 2012, 2013). Several examples of spectral TDIP applications have been presented, for landfill delineation (Gazoty *et al.*, 2012b, 2013; Wemegah *et al.*, 2016), lithotype characterization (Chongo *et al.*, 2015; Gazoty *et al.*, 2012a; Johansson *et al.*, 2015, 2016; Maurya *et al.*, 2016), time-lapse monitoring of CO_2 injection (Doetsch *et al.*, 2015a) and freezing of active layer in permafrost (Doetsch *et al.*, 2015b). Furthermore, efforts have been made to achieve a wider time-range in TDIP acquisition, up to four decades in time (Olsson *et al.*, 2016), for enhanced spectral content. In this work a review of the recent advances in spectral inversion of TDIP data is presented, in terms of: supported IP parameterizations; modelling of transmitter waveform; support for buried electrodes; model regularization; computation of the depth of investigation.

ADVANCES IN SPECTRAL TDIP INVERSION

In the spectral inversion of TDIP data, the data space is composed by the apparent resistivity and the full voltage decays, while the model space is constituted by a parameterization of IP. The Cole-Cole model (Cole-Cole, 1941; Pelton *et al.*, 1978) and the Constant Phase Angle (CPA) model (Van Voorhis *et al.*, 1973) are the two parameterizations currently implemented in AarhusInv (Auken *et al.*, 2015), the software in which the inversion algorithms described in Fiandaca *et al.* (2012,2013) are implemented. The complex resistivity $\zeta_{Cole\text{-}Cole}$ of the Cole-Cole model takes the form:

$$\zeta_{Cole-Cole} = \rho\left(1 - m_0\left(1 - \frac{1}{1 + (i\omega\tau)^C}\right)\right) \qquad (1)$$

where ρ is the direct current resistivity, m_0 is the intrinsic chargeability, τ is the time constant, C is the frequency exponent and i is the imaginary unit. The complex resistivity ζ_{CPA} of CPA model is expressed as:

$$\zeta_{CPA} = K(i\omega)^{-b} \qquad (2)$$

where b is a positive fraction, $\varphi = -\frac{\pi}{2}b$ represents the phase shift and defines completely the IP response, K is a constant and i is the imaginary unit. In the CPA model, the DC resistivity cannot be defined, because the complex resistivity increases indefinitely at low frequencies. For this reason, Van Voorhis *et al.* (1973) introduced the Drake model:

$$\zeta_{Drake} = K(i\omega + \omega_L)^{-b} \qquad (3)$$

where in comparison with the CPA model a low frequency pole ω_L is introduced and the DC resistivity can be defined as $\rho = K{\omega_L}^{-b}$. In the AarhusInv implementation of the time-domain CPA forward response the Drake model of equation (3) is actually used, with a fixed value for the low frequency pole $\omega_L = 10^{-5}$ Hz. In this way, the CPA inversion is set up in terms of the model parameters ρ and φ, while the Cole-Cole inversion is set up in terms of ρ, m_0, τ and C. Considering that the CPA and the Cole-Cole models are easily distinguishable in time-domain when more than 2 orders of magnitudes are acquired in the time-range (Lajaunie *et al.*, 2016), the choice between the different supported IP parameterizations can be driven by the actual spectral content of the data. For both models it is also possible to invert directly for the normalized chargeability parameters φ/ρ or m_0/ρ, instead of φ or m_0.

The forward modelling in AarhusInv, whatever parameterization is used for IP, takes into account the transmitter waveform and the receiver transfer function (Figure 1), for an accurate modelling of the IP response (Fiandaca *et al.*, 2012,2013). The inversion is performed iteratively, by using the first term of the Taylor expansion of the nonlinear forward mapping of the model to the data space, as described in details in Auken *et al.* (2015). Figure 2 shows two typical forward responses for Cole-Cole and CPA homogeneous half spaces. The shape of the decays contains the spectral information of the IP phenomenon, which can be properly retrieved when the transmitter/receiver characteristics are properly modelled (Fiandaca *et al.*, 2012; Fiandaca *et al.*, 2013; Lajaunie *et al.*, 2016; Madsen *et al.*, 2016). Recently, the modelling of the IP response during the current on-time with a 100% duty cycle transmitter waveform has been implemented in AarhusInv (Figure 3). With the 100% duty cycle the current switches directly from positive to negative values, allowing for shorter acquisition times (because the off-time is skipped) and better signal-to-noise ratio (because the measured voltages are higher for the 100% duty cycle), but keeping equivalent spectral content when compared to the

50% duty cycle waveform (Olsson *et al.*, 2015; Madsen *et al.*, 2016).

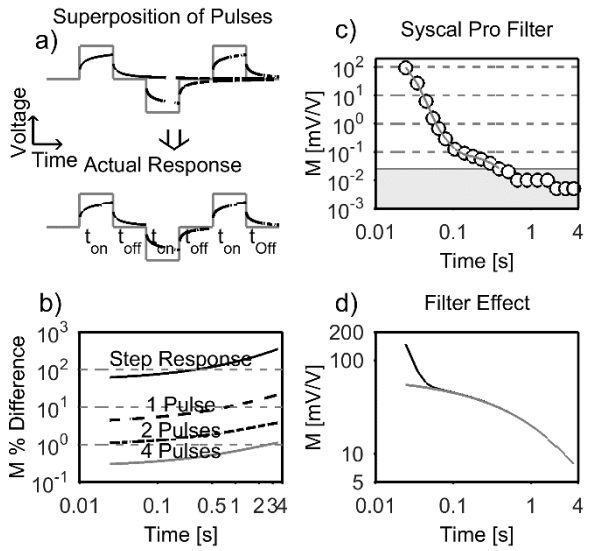

Figure 1 (after Fiandaca et al, 2013). (a) Construction of the actual response by superimposing step responses; (b) IP percentage difference between decays with different number of stacks (a decay stacked six times is used as a reference) for the homogeneous half-space described by the Cole–Cole parameters (m_0 = 100 mV/V, τ =2 s, C=0.5). (c) IRIS Syscal Pro filter effect (circles) measured in the time domain on a non-chargeable resistor. (d) Example of forward response with the filter implementation (black line) and without the filter implementation (grey line).

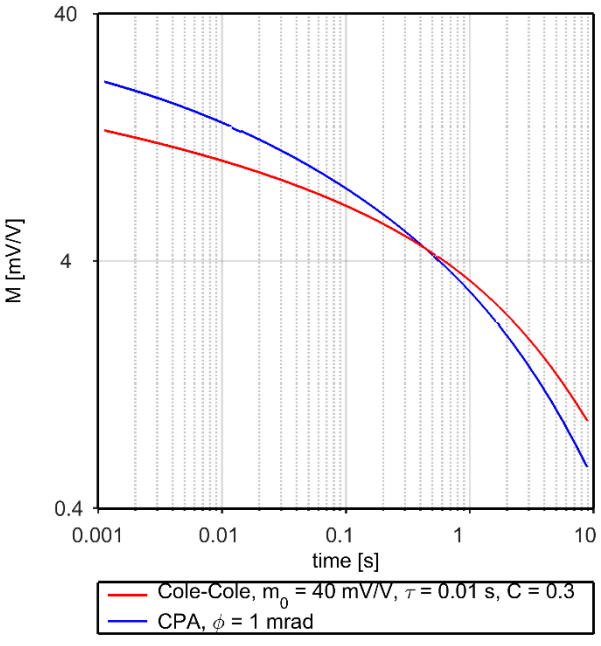

Figure 2. Examples of Cole-Cole decay (red curve) and CPA decay (blue curve) for homogeneous half spaces and 50% duty cycle waveform (T_{on}= T_{off} =10 s, 4 stacked pulses).

In addition to the 1-D and 2-D implementations described in Fiandaca *et al.* (2012,2013), the IP forward modelling in AarhusInv has been recently enriched by the possibility of computing the response for buried electrodes, for inversion of 1-D borehole and 2-D cross-borehole data. The 1-D implementation computes the kernel following Sato (2000), with recursion formulas over the layers. Considering that in borehole data often hundreds of layers are modelled (Auken *et al.*, 2016), the lateral-constrained approach has been implemented for speeding-up computations. The full 1-D model containing hundreds of layers is split into several sub-models containing only a few tens of layers and the data are subdivided in subsets grouped by pseudodepth.

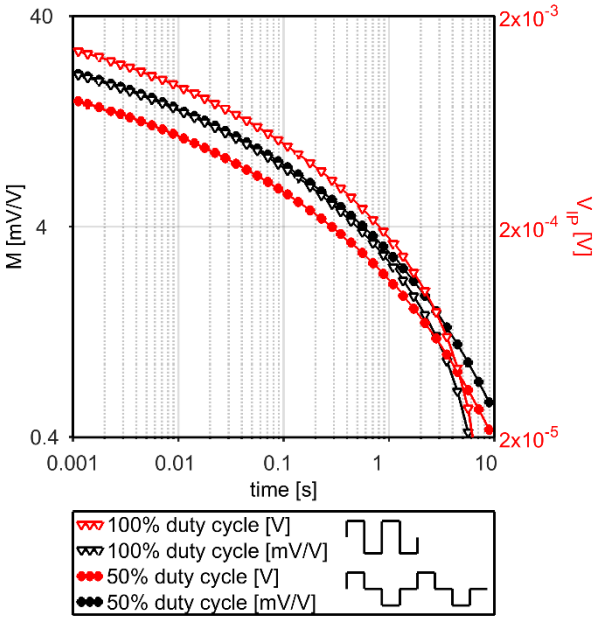

Figure 3. 50% duty cycle decays (circles) and 100% duty cycle decays (triangles) for Cole-Cole homogeneous halfspace (ρ=100 Ωm, m_0=40 mV/V, τ=0.01 s, C=0.3, T_{on}/T_{off} =10 s, 4 stacked pulses). Black lines represent the normalized decays in mV/V, while red lines represent the actual voltages (see Olsson *et al.* (2015) for details).

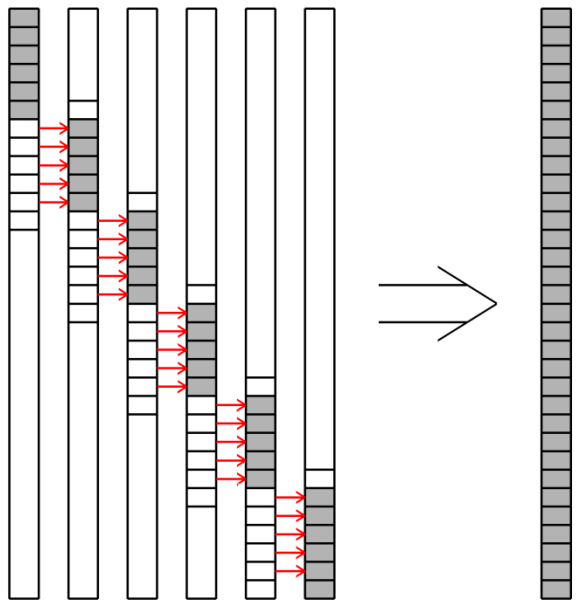

Figure 4. Split of a 32-layers 1D model (grey model) in six 13-layers laterally-constrained sub-models for computational efficiency. The red arrows represent the lateral constraints.

The inversion is then carried out in parallel on the split sub-models/datasets and the full model is reconstructed stitching together the sub-models after inversion (Figure 4). This approach allows for gaining more than two order of magnitudes in run-time. The 2-D cross-hole computation has been implemented simply allowing the electrodes to be positioned at any node (on the surface or buried) of the finite-element mesh (Bording *et al.*, 2016).

Compared to the implementations presented in Fiandaca *et al.* (2012,2013), new regularization schemes have been implemented for the spectral inversion of TDIP data, for vertical/horizontal constraints that favour sharp models (Vignoli *et al.*, 2015) and for time-lapse constraints that promote compact time-lapse changes (Fiandaca *et al.*, 2015a). In particular, two generalizations of the minimum support norm, namely $\varphi_{symmetric}$ and $\varphi_{asymmetric}$, have been developed for time-lapse inversion:

$$\varphi_{symmetric}(x) = \alpha^{-1}\frac{(x^2/\sigma^2)^p}{(x^2/\sigma^2)^p + 1} \quad (4)$$

$$\varphi_{asymmetric} = \alpha^{-1}\left[(1-\beta)\cdot\frac{(x^2/\sigma^2)^{p_1}}{(x^2/\sigma^2)^{p_1}+1} + \beta\cdot\frac{(x^2/\sigma^2)^{p_2}}{(x^2/\sigma^2)^{p_2}+1}\right] \quad (5a)$$

$$\beta = \frac{(x^2/\sigma^2)^{max(p_1,p_2)}}{(x^2/\sigma^2)^{max(p_1,p_2)}+1} \quad (5b)$$

where: $x = m - m_0$ represents the difference between the reference value and the updated value in the time-lapse inversion for a given model parameter, i.e. the time-lapse change; σ represents the transition point of the minimum functional φ and controls the sharpness of time-lapse changes; α controls the relative weight of data and model measures in the objective function and affects the size of time-lapse changes; p (or p_1 and p_2) controls the transition sharpness of φ (Figure 5) and determines the way in which the overall focusing depends on σ and α (Fiandaca *et al.*, 2015a).

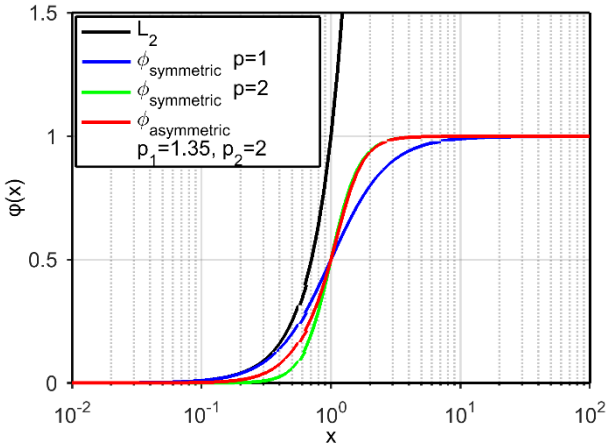

Figure 5. Comparison of L₂ norm, symmetric minimum support (equation 4) and asymmetric minimum support (equation 5) with varying norm settings.

With the classic L2 norm $\varphi_{L_2}(x) = x^2/\sigma^2$, the penalty in the objective function for a time-lapse change $x = m - m_0$ increases with the square of x. With the norms of equation 4 and equation 5 the penalty does not increase indefinitely with x, but reaches a maximum when $x \gg \sigma$ (Figure 5). This favours compact time-lapse changes, and the compactness can be easily and predictably controlled through the σ, α and p settings. In many time-lapse experiments diffusive processes are monitored, and compact time-lapse changes do not necessarily represent the underlying physics/geochemistry. However, robust and easy-to-tune regularizations that favour the smallest model variation compatible with the data can be a very helpful tool for data interpretation, when used together with model measures that promote smooth variations.

Finally, a new robust concept for the calculation of the depth of investigation (DOI) for inversion problems described by several intrinsic parameters, like the spectral inversion of time-domain induced polarization data, has been developed (Fiandaca *et al.*, 2015b). A calculation of the DOI is crucial for interpreting the geophysical models, as the validity of the model varies considerably with data noise and parameter distribution. Without the DOI estimate, it is difficult to judge when the information in the model is data-driven or is strongly dependent on the constraints and/or on the starting value. The proposed method is based on an approximated covariance analysis applied to the model output from the inversion while considering the data standard deviations. Furthermore, the cross-correlations between intrinsic parameters are taken into account in the computations, which is crucial when strong cross-correlations are expected. Our new DOI implementation starts by subdividing the 2-D section in $[N_{Layers} \times N_{columns}]$ cells, and summing the Jacobian elements of the $N_{columns}$ model columns downwards. For each layer n and each model column l a cumulated $[N_{Data} \times N_{Par}]$ quasi-Jacobian matrix is defined (cumulated downward from the n^{th} layer to the last layer):

$$G_{Cum}^{n,l}(i,k) := \sum_{j=j_{k,l}-n+1}^{j_{k,l}} G(i,j) \quad (6)$$

$$\forall i \in [1, N_{Data}], \forall k \in [1, N_{Par}],$$

$$\forall n \in [1, N_{Layers}], \forall l \in [1, N_{Columns}]$$

where $j_{k,l}$ represents the model index of the k^{th} parameter of the last layer of the l^{th} model column, N_{Data} is the number of data, N_{Par} is the number of intrinsic parameters (e.g. 4 for the Cole-Cole model), N_{Layers} is the number of layers in the 2-D model and $N_{Columns}$ is the number of model columns in the 2-D model. It is then possible to define a $[N_{Par} \times N_{Par}]$ cumulated approximate analysis for each model column l and each layer n of the 2D section:

$$\boldsymbol{CAA}^{n,l} := \left[\left(\boldsymbol{G}_{Cum}^{n,l}\right)^T \boldsymbol{C}_d{}^{-1}\left(\boldsymbol{G}_{Cum}^{n,l}\right)\right]^{-1} \quad (7)$$

The cumulated approximate analysis $\boldsymbol{CAA}^{n,l}$ corresponding to the n^{th} layer does not contain information on the parameters of the n^{th} layer alone, but it cumulates the sensitivity from the n^{th} layer down to the last layer. This means that the cumulated approximate analysis gives information on all the layers below the n^{th} layer at once, for each model column l. In equation 7 the correlation between model parameters

belonging to different model columns are neglected (lateral data correlation), but the correlation among the N_{Par} intrinsic parameters for each model column is considered. The inversion is carried out in logarithmic model space, and thus we use a standard deviation factor, $STDF$, for each parameter k:

$$STDF^{n,l}(k) := exp\left(\sqrt{CAA^{n,l}(k,k)}\right) \quad (8)$$

The DOI-value is then defined for each parameter k and each model column l by imposing a threshold value for the $STDF$, bearing the implicit meaning that below this threshold the model structures are not data driven, but rather a result of the constraints and/or inversion properties. Figure 6 shows the $STDF$ values and the corresponding DOI computations for a typical 3-layers Cole-Cole model for a Schlumberger sounding (red lines). Furthermore, the results when disregarding the off-diagonal elements in $\left(\boldsymbol{G}_{Cum}^{n,l}\right)^T \boldsymbol{C}_d{}^{-1}\left(\boldsymbol{G}_{Cum}^{n,l}\right)$, i.e. the parameter correlations, are presented (blue lines): the DOI is significantly overestimated when neglecting the parameter correlations.

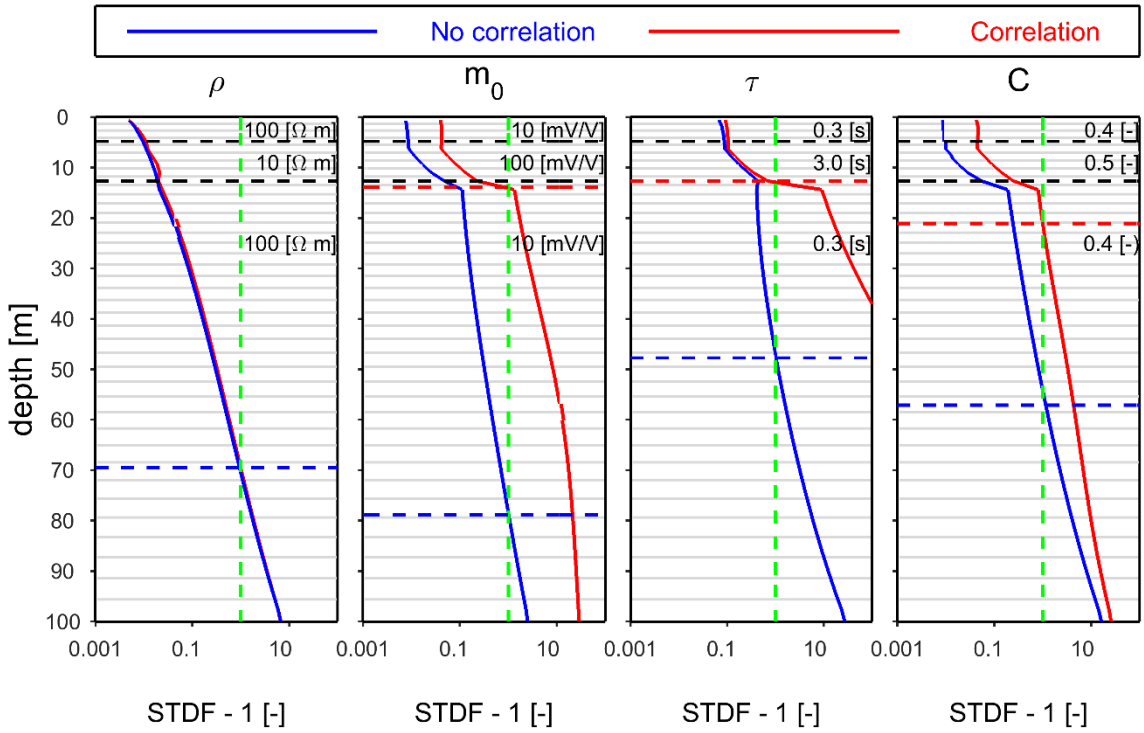

Figure 6. Depth of investigation (DOI) for an exemplary 3-layers Cole-Cole model for a Schlumberger sounding. Black dashed lines: layer interfaces. Continuous grey lines: vertical model subdivision for the *STDF* computation (equation 8) as a function of depth. Green dashed lines: threshold value for the *STDF* computation. Red lines: *STDF* values as a function of depth taking into account the parameter correlations (continuous lines) and corresponding DOI values (dashed lines). Blue lines: *STDF* values as a function of depth disregarding the parameter correlations (continuous lines) and corresponding overestimated DOI values (dashed lines).

CONCLUSIONS

The spectral inversion of TDIP data has reached maturity. Different IP parameterizations can be modelled, i.e. the Cole-Cole and the CPA models, and the choice between the models can be made in function of the actual spectral content of the data. The forward modelling takes into account the transmitter waveform and the receiver transfer function for accurate computations, and the 100% duty cycle is supported for shorted acquisition time and better signal-to-noise ratio. Computation with buried electrodes for 1-D and 2-D modelling has been implemented, and advanced model regularizations have been developed, for sharp vertical/horizontal model variations and compact changes in time-lapse inversion. Furthermore, a new robust concept for the calculation of the depth of investigation has been developed, enabling judging when the information in the model is data-driven or is strongly dependent on the constraints and/or on the starting value. We believe that the advances in spectral TDIP inversion significantly increase the potential of TDIP in (hydro)geophysical applications.

ACKNOWLEDGMENTS

Support was provided by the research project GEOCON, Advancing GEOlogical, geophysical and CONtaminant monitoring technologies for contaminated site investigation (contract 1305-00004B). The funding for GEOCON is provided by The Danish Council for Strategic Research under the Programme commission on sustainable energy and environment.

REFERENCES

Auken E., Christiansen A.V., Kirkegaard C., Fiandaca G., Schamper C., Behroozmand A.A., Binley A., Nielsen E., Efferso F., Christensen N.B., Sorensen K., Foged N. & Vignoli G., 2015. An overview of a highly versatile forward and stable inverse algorithm for airborne, ground-based and borehole electromagnetic and electric data, Exploration Geophysics, 46, 223-235. 10.1071/eg13097.

Auken E., Fiandaca G., Christiansen A.V., Maurya P.K., Holm H., 2016. Mapping lithotypes using in-situ measurement of time domain induced polarization: El-log. 4th IP Workshop, 6-8 June 2016, Aarhus, Denmark.

Bording T.S., Fiandaca G., Maurya P.K., Auken E., Christiansen A.V., 2016. Mapping possible flowpaths of contaminants through surface and cross-borehole spectral time-domain induced polarization. 4th IP Workshop, 6-8 June 2016, Aarhus, Denmark.

Chongo M., Christiansen A.V., Fiandaca G., Nyambe I.A., Larsen F. & Bauer-Gottwein P., 2015. Mapping localised freshwater anomalies in the brackish paleo-lake sediments of the Machile-Zambezi Basin with transient electromagnetic sounding, geoelectrical imaging and induced polarisation, Journal of Applied Geophysics, 123, 81-92. 10.1016/j.jappgeo.2015.10.002.

Cole K.S., Cole R.H., 1941. Dispersion and absorption in dielectrics I. Alternating current characteristics. J. Chem. Phys. 9 (4), 341.

Doetsch J., Ingeman-Nielsen T., Christiansen A.V., Fiandaca G., Auken E. & Elberling B., 2015a. Direct current (DC) resistivity and induced polarization (IP) monitoring of active layer dynamics at high temporal resolution, Cold Regions Science and Technology, 119, 16-28. 10.1016/j.coldregions.2015.07.002.

Doetsch J., Fiandaca G., Auken E., Christiansen A.V., Cahill A.G. & Jakobsen R., 2015b. Field-scale time-domain spectral induced polarization monitoring of geochemical changes induced by injected CO2 in a shallow aquifer, Geophysics, 80, WA113-WA126. 10.1190/geo2014-0315.1.

Fiandaca G., Auken E., Christiansen A.V. & Gazoty A., 2012. Time-domain-induced polarization: Full-decay forward modeling and 1D laterally constrained inversion of Cole-Cole parameters, Geophysics, 77, E213-E225. 10.1190/geo2011-0217.1.

Fiandaca G., Ramm J., Binley A., Gazoty A., Christiansen A.V. & Auken E., 2013. Resolving spectral information from time domain induced polarization data through 2-D inversion, Geophysical Journal International, 192, 631-646. 10.1093/gji/ggs060.

Fiandaca G., Doetsch J., Vignoli G. & Auken E., 2015a. Generalized focusing of time-lapse changes with applications to direct current and time-domain induced polarization inversions, Geophysical Journal International, 203, 1101-1112. 10.1093/gji/ggv350.

Fiandaca G., Christiansen A. & Auken E., 2015b. Depth of Investigation for Multi-parameters Inversions, Near Surface Geoscience 2015-21st European Meeting of Environmental and Engineering Geophysics, 1-4. 10.3997/2214-4609.201413797.

Gazoty A., Fiandaca G., Pedersen J., Auken E., Christiansen A.V. & Pedersen J.K., 2012a. Application of time domain induced polarization to the mapping of lithotypes in a landfill site, Hydrology and Earth System Sciences, 16, 1793-1804. 10.5194/hess-16-1793-2012.

Gazoty A., Fiandaca G., Pedersen J., Auken E. & Christiansen A.V., 2012b. Mapping of landfills using time-domain spectral induced polarization data: the Eskelund case study, Near Surface Geophysics, 10, 575-586. 10.3997/1873-0604.2012046.

Gazoty A., Fiandaca G., Pedersen J., Auken E. & Christiansen A.V., 2013. Data repeatability and acquisition techniques for time-domain spectral induced polarization, Near Surface Geophysics, 11, 391-406. 10.3997/1873-0604.2013013.

Johansson S., Fiandaca G. & Dahlin T., 2015. Influence of non-aqueous phase liquid configuration on induced polarization parameters: Conceptual models applied to a time-domain field case study, Journal of Applied Geophysics, 123, 295-309. 10.1016/j.jappgeo.2015.08.010.

Johansson S., Sparrenbom C., Fiandaca G., Olsson P.-I., Dahlin T. & Rosqvist H., 2016. Investigations of a Cretaceous limestone with spectral induced polarization and scanning electron microscopy, Geophysical Journal International, Under Review.

Lajaunie M., Maurya P.K., Fiandaca G., 2016. Comparison of Cole-Cole and Constant Phase Angle modeling in time-domain induced polarization. 4th IP Workshop, 6-8 June 2016, Aarhus, Denmark.

Madsen L.M., Kirkegaard C., Fiandaca G., Christiansen A.V., Auken E., 2016. An analysis of Cole-Cole parameters for IP data using Markov chain Monte Carlo. 4th IP Workshop, 6-8 June 2016, Aarhus, Denmark.

Maurya P.K., Fiandaca G., Auken E., Christiansen A.V., 2016. Lithological characterization of a contaminated site using Direct current resistivity and time domain Induced Polarization. 4th IP Workshop, 6-8 June 2016, Aarhus, Denmark.

Olsson P.-I., Dahlin T., Fiandaca G. & Auken E., 2015. Measuring time-domain spectral induced polarization in the on-time: decreasing acquisition time and increasing signal-to-noise ratio, Journal of Applied Geophysics, 123, 316-321. 10.1016/j.jappgeo.2015.08.009.

Olsson P.I., Fiandaca G., Larsen J.J., Dahlin T., Auken E., 2016. Doubling the spectrum of time-domain induced polarization: removal of non-linear self-potential drift, harmonic noise and spikes, tapered gating, and uncertainty estimation. 4th IP Workshop, 6-8 June 2016, Aarhus, Denmark.

Pelton W.H., Ward S.H., Hallof P.G., Sill W.R., Nelson P.H., 1978. Mineral discrimination and removal of inductive coupling with multifrequency IP. Geophysics 43 (3), 588–609.

Sato H.K., 2000. Potential field from a dc current source arbitrarily located in a nonuniform layered medium. Geophysics, 65 (6), 1726–1732.

Van Voorhis G.D., Nelson P.H., Drake T.L., 1973. Complex resistivity spectra of porphyry copper mineralization. Geophysics 38 (1), 49–60

Vignoli G., Fiandaca G., Christiansen A.V., Kirkegaard C. & Auken E., 2015. Sharp spatially constrained inversion with applications to transient electromagnetic data, Geophysical Prospecting, 63, 243-255. 10.1111/1365-2478.12185.

Wemegah D.D., Fiandaca G., Auken E., Menyeh A. & Danuor S.K., 2016. Spectral time-domain induced polarization and magnetic surveying – an efficient tool for characterization of solid waste deposits in developing countries, Near Surface Geophysics, Under Review.